

# Production of cosmogenic isotopes $^7\text{Be}$ , $^{10}\text{Be}$ , $^{14}\text{C}$ , $^{22}\text{Na}$ and $^{36}\text{Cl}$ in the atmosphere: Altitudinal profiles of yield functions

S. Poluianov,<sup>1</sup> G.A. Kovaltsov,<sup>2</sup> A.L. Mishev,<sup>1</sup> I.G. Usoskin,<sup>1,3</sup>

## Key points.

- A new consistent set of yield functions for cosmogenic isotopes  $^7\text{Be}$ ,  $^{10}\text{Be}$ ,  $^{14}\text{C}$ ,  $^{22}\text{Na}$ ,  $^{36}\text{Cl}$  by cosmic rays in the atmosphere is presented.
- For the first time, a detailed altitudinal profile of the production is given.
- The results can be straightforwardly used in the atmospheric chemistry and dynamics models.

---

Corresponding author: I. Usoskin University of Oulu, Finland, (ilya.usoskin@oulu.fi)

<sup>1</sup>ReSoLVE Center of Excellence,  
University of Oulu, Finland.

<sup>2</sup>Ioffe Physical-Technical Institute of  
Russian Academy of Sciences, St.  
Petersburg, Russia.

<sup>3</sup>Sodankylä Geophysical Observatory  
(Oulu unit), University of Oulu, Finland.

**Abstract.** New consistent and precise computations of the production of five cosmogenic radio-isotopes,  $^7\text{Be}$ ,  $^{10}\text{Be}$ ,  $^{14}\text{C}$ ,  $^{22}\text{Na}$  and  $^{36}\text{Cl}$ , in the Earth's atmosphere by cosmic rays are presented in the form of tabulated yield functions. For the first time, a detailed set of the the altitude profiles of the production functions is provided which makes it possible to apply the results directly as input for atmospheric transport models. Good agreement with most of the earlier published works for columnar and global isotopic production rates is shown. Altitude profiles of the production are important, in particular for such tasks as studies of strong solar particle events in the past, precise reconstructions of solar activity on long-term scale, tracing air-mass dynamics using cosmogenic radio-isotopes, etc. As an example, computations of the  $^{10}\text{Be}$  deposition flux in the polar region are shown for the last decades and also for a period around 780 AD and confronted with the actual measurements in Greenland and Antarctic ice cores.

## 1. Introduction

Earth is permanently bombarded by high-energy nucleonic particles – cosmic rays, which produce nucleonic-muon-electromagnetic cascades in the Earth’s atmosphere. As a sub-product of the cascade, radioactive isotopes can be produced, called cosmogenic nuclides. Measurements of the abundance of long-living cosmogenic radionuclides in the atmosphere and terrestrial archives (ice cores, tree trunks, sediments, etc.) form a very important tool to study atmospheric processes and interaction between different reservoirs (see, e.g., books by *Dorman* [2004] and *Beer et al.* [2012]). This also offers a reliable quantitative method to study solar activity on the long time scale [*McCracken et al.*, 2004; *Solanki et al.*, 2004; *Vonmoos et al.*, 2006; *Muscheler et al.*, 2007; *Steinhilber et al.*, 2012; *Inceoglu et al.*, 2015; *Usoskin*, 2013; *Usoskin et al.*, 2014]. Most important for these purposes are cosmogenic isotopes  $^7\text{Be}$  (half-life  $\approx 53$  days),  $^{22}\text{Na}$  (2.6 years),  $^{14}\text{C}$  (5730 years),  $^{36}\text{Cl}$  ( $3 \cdot 10^5$  years) and  $^{10}\text{Be}$  ( $1.4 \cdot 10^6$  years), and many studies are based on these data.

Although the relation between cosmic ray variability and cosmogenic isotopes is qualitatively obvious, their quantitative modelling is difficult, since they are produced in complex atmospheric cascades which require extensive computations. First numerical models of cosmogenic nuclide production were developed already in the 1960–1970s [e.g. *Lal and Peters*, 1962; *Lingenfelter*, 1963; *O’Brien*, 1979], using either direct modelling or (semi)empirical parameterizations. A benchmark was achieved by *Masarik and Beer* [1999] (updated as *Masarik and Beer* [2009]) who applied modern high-performance computers for direct Monte-Carlo simulations of the atmospheric cascade to model production rates of isotopes  $^7\text{Be}$ ,  $^{10}\text{Be}$ ,  $^{14}\text{C}$  and  $^{36}\text{Cl}$ . Unfortunately, their computations were made

for a prescribed spectrum of cosmic rays without the yield-function approach (see Sect. 2). This shortcoming was soon overcome in a number of original works presenting production yield functions for different isotopes: *Webber and Higbie* [2003] and *Webber et al.* [2007] calculated yield functions for  $^7\text{Be}$ ,  $^{10}\text{Be}$  and  $^{36}\text{Cl}$  using FLUKA Monte-Carlo code [Fassò et al., 2001]; *Usoskin and Kovaltsov* [2008], *Kovaltsov and Usoskin* [2010] and *Leppänen et al.* [2012] calculated, using the CRAC (Cosmic Ray induced Atmospheric Cascade) model, based on CORSIKA Monte-Carlo tool [Heck et al., 1998], yield functions for cosmogenic  $^7\text{Be}$ ,  $^{10}\text{Be}$  and  $^{22}\text{Na}$ , respectively; the yield function for production of  $^{14}\text{C}$  was calculated by *Kovaltsov et al.* [2012] using the GEANT4-based tool PLANETOCOSMICS [Desorgher et al., 2009]. Thus, it is presently a mixture of different yield functions calculated by different models with different assumptions and conditions.

For many tasks it is important to know detailed altitude profiles of the isotope production: studies of solar energetic particle events in the past [e.g., *Usoskin et al.*, 2006; *Webber et al.*, 2007; *Miyake et al.*, 2012; *Usoskin et al.*, 2013]; detailed reconstructions of long-term solar activity using isotopes of  $^{10}\text{Be}$  and  $^{36}\text{Cl}$  including realistic atmospheric transport [e.g., *McCracken*, 2004; *Field et al.*, 2006; *Pedro et al.*, 2006; *Heikkilä et al.*, 2009; *Delaygue et al.*, 2015]; in situ atmospheric measurements of  $^{14}\text{C}$  [*Jöckel et al.*, 1999, 2003; *Kanu et al.*, 2016]; tracing of air-mass dynamics and water flows using cosmogenic radioisotopes [e.g., *Jordan et al.*, 2003; *Sakaguchi et al.*, 2005; *Leppänen et al.*, 2012; *Ioannidou and Paatero*, 2014; *Pacini et al.*, 2015]. However, the previously published yield functions were presented either without altitudinal resolution, giving only atmospheric columnar or global production of isotopes, or with very rough altitudinal resolution, insufficient for detailed computations. This made it difficult to solve the above tasks independently with-

out involving modelling groups making additional laborious detailed simulations. While *Masarik and Beer* [1999] provided computations with a detailed vertical resolution, they were not based on the yield-function formalism, limited to a prescribed energy spectrum of GCR, thus being inapplicable to, e.g., an analysis of solar energetic particle events. Moreover, they included  $\alpha$ - and heavier particles as scaled protons, which is not exactly correct [Webber *et al.*, 2007].

Here we present a new computation of yield functions for a set of widely used cosmogenic isotopes, viz.  $^7\text{Be}$ ,  $^{10}\text{Be}$ ,  $^{14}\text{C}$ ,  $^{22}\text{Na}$  and  $^{36}\text{Cl}$ , in the Earth's atmosphere. These isotopes are produced in the atmosphere in nuclear reactions on nitrogen, oxygen and argon, induced by nucleonic particles (neutrons, protons and  $\alpha$ -particles) of the nucleonic cascade. We provide a set of new consistent computations of the yield function production for cosmogenic isotopes, using one and the same Monte-Carlo model (GEANT4) with fixed physical sub-model options, atmospheric parameters and basic assumptions, and assess uncertainties arising. For the first time, we publish (see the Supporting information) a detailed set of altitude profiles of production functions of the cosmogenic isotopes making it possible for everyone to calculate the full 3D atmospheric production of isotopes.

## 2. Yield function: Formalism and computational model

### 2.1. Formalism

A standard approach to model various effects of cosmic rays in the atmosphere, including production of cosmogenic isotopes, is based on the yield function formalism.

The yield function,  $Y(E, h)$ , is defined as the production (the number of atoms per gram of air) of the isotope, at given atmospheric depth  $h$ , by primary particles of type  $i$  with the unit intensity (one primary particle with kinetic energy per nucleon  $E$  in the

interplanetary space per steradian and  $\text{cm}^2$ ). The units of  $Y$  are  $[\text{atoms g}^{-1} \text{ cm}^2 \text{ sr}]$ . The production rate  $Q$  of cosmogenic isotope at time  $t$  is then defined as an integral of the product of the yield function and the energy spectrum of cosmic rays  $J_i(E, t)$   $[\text{sr sec cm}^2]^{-1}$ ), above the energy  $E_c$  corresponding to the local geomagnetic rigidity cutoff  $P_c$ :

$$Q(t, h, P_c) = \sum_i \int_{E_{c,i}}^{\infty} Y_i(E, h) \cdot J_i(E, t) \cdot dE, \quad (1)$$

where the summation is over different types of primary cosmic ray particles (protons,  $\alpha$ -particles, etc.). The relation between  $E_{c,i}$  and  $P_c$  (defined independently of the yield function computations) is

$$E_{c,i} = E_r \cdot \left( \sqrt{1 + \left( \frac{Z_i \cdot P_c}{A_i \cdot E_r} \right)^2} - 1 \right), \quad (2)$$

where  $Z_i$  and  $A_i$  are the charge and mass numbers of particles, respectively,  $E_r = 0.938$  GeV is the rest mass of a proton. For computations of the yield function we considered, as primary particles, only protons and  $\alpha$ -particles. Species heavier than helium can be effectively considered as scaled (by the nucleonic number)  $\alpha$ -particles [see *Webber and Higbie, 2003*]. An advantage of this approach is that the production rate can be calculated for any type of the energy spectrum beyond the standard modulated spectrum of galactic cosmic rays (GCR), for example, for solar energetic particle events or hypothetical nearby supernova explosions. Sometimes production of cosmogenic isotopes is calculated directly, without the yield function [*O'Brien, 1979; Masarik and Beer, 1999; Masarik and Beer, 2009*], but this is related to a prescribed cosmic-ray spectrum and cannot be applied for a different or/and revised spectrum.

We note that the computational results are often given not as the strictly defined yield function  $Y$  (see above) but the so-called ‘production function’  $S$ , which gives production

of the cosmogenic isotope per one primary particle impinging on the top of the atmosphere [e.g., *Webber et al.*, 2007]. Here we show and tabulate the production function  $S$  which is a direct result of the simulations and which is related, for the isotropic flux of primary cosmic rays, to the true yield function as

$$Y = \pi S. \quad (3)$$

The factor  $\pi$  appears as conversion between the flux on the top of the atmosphere and the CR intensity in the interplanetary space [cf., e.g., *Grieder*, 2001, Chapter 1.6.2].

## 2.2. Numerical calculation of the yield function

Simulations of the nucleonic cascade in the atmosphere were made using direct Monte-Carlo simulations by the general-purpose toolkit GEANT4 10.0 developed in CERN for modelling the particle transport and interactions [*Agostinelli et al.*, 2003; *Allison et al.*, 2006]. For our task we applied the embedded physics list QGSP\_BIC\_HP (Quark-Gluon String model for high-energy interactions + Geant4 Binary Cascade + High-Precision neutron package) [*GEANT4 collaboration*, 2013]. The Earth’s atmosphere was modelled in a realistic manner as a set of spherical layers with homogeneous properties according to the empirical model of the atmosphere NRLMSISE-00 [*Picone et al.*, 2002]. The top of the model was set at the altitude of 100 km, and the layers had the thickness from 1 g/cm<sup>2</sup> (for the top 20 g/cm<sup>2</sup>) to 10 g/cm<sup>2</sup> (for the ones below 20 g/cm<sup>2</sup>). The total depth of the atmosphere was set to 1050 g/cm<sup>2</sup>, and the soil was not included into the model.

The primary cosmic rays were modelled, in each simulation, as the monoenergetic (viz. with a fixed energy) isotropic flux impinging on the top of the atmosphere. We did a series of simulations for two types of cosmic rays, primary protons and  $\alpha$ -particles with fixed

energies in the range from 20 MeV/nuc to 100 GeV/nuc with a quasi-logarithmically distributed values. We note that the computations are presented not for energy bins but for the fixed energies as denoted in the supplement information Tables. From these simulations, the depth-energy distributions of the fluxes of cascade particles (protons, neutrons and  $\alpha$ -particles, both primaries and secondaries) were stored as histograms with energy range 1 keV – 100 GeV with logarithmic bins in energy (20 bins per decade).

We obtained sums of simulated secondary particles with their energy binned into energy bins of width  $\Delta E'$  centered at the energy  $E'$ , that have crossed a given horizontal level (atmospheric depth,  $h$ ), and applying a weight of  $|\cos \theta|^{-1}$  (where  $\theta$  is the zenith angle of the secondaries) to account for the geometrical factor. The minimum value of  $|\cos \theta|$  was limited to 0.001 to avoid too high weights. These sums were divided by the energy bin width  $\Delta E'$  to correspond to the quantity  $F_k(E', h)$  which is defined as

$$F_k(E', h) \equiv N_k(E', h) v_k(E'), \quad (4)$$

where  $N_k$  and  $v_k$  are the concentration (in  $[\text{MeV cm}^3]^{-1}$ ) and velocity of secondary particles of type  $k$  with energy  $E'$  at the atmospheric depth level  $h$ . Then the production function  $S$  (in units of atoms/g) at the given atmospheric level  $h$  is defined as

$$S(E, h) = \sum_j \sum_k \int \kappa_j \cdot F_k(E', h) \cdot \sigma_{j,k}(E') \cdot dE' \quad (5)$$

where  $\kappa_j$  is the content of the target nuclei in one gram of air (atoms/g),  $\sigma_{j,k}$  is the cross-section of the corresponding nuclear reactions, and summation is over the type of secondary particle  $k$  and the type  $j$  of the target nucleus.

Radiocarbon  $^{14}\text{C}$  is produced mostly via capture of secondary neutrons by atmospheric nitrogen which composes 78% of the atmosphere by volume. The  $^7\text{Be}$  and  $^{10}\text{Be}$  isotopes



are produced by spallation of atmospheric nitrogen and oxygen (forming together about 99% of the atmosphere by volume). The  $^{22}\text{Na}$  and  $^{36}\text{Cl}$  isotopes are produced by spallation of atmospheric argon (about 1% of the atmosphere by volume) which is much less abundant than nitrogen and oxygen. In computations we adopted the cross sections from *Reyss et al.* [1981]; *Lange et al.* [1995]; *Jull et al.* [1998]; *Webber and Higbie* [2003]; *Tatischeff et al.* [2006]; *Beer et al.* [2012] and also from the Experimental Nuclear Reaction Database (EXFOR/CSISRS) <http://www.nndc.bnl.gov/exfor/exfor00.htm>. We note that cross-sections we used to compute the production of  $^7\text{Be}$ ,  $^{10}\text{Be}$ ,  $^{14}\text{C}$  and  $^{22}\text{Na}$  are the same as in our previous works [*Usoskin and Kovaltsov*, 2008; *Kovaltsov and Usoskin*, 2010; *Kovaltsov et al.*, 2012; *Leppänen et al.*, 2012]. Transport of neutrons with energy below 1 keV, for production of  $^{14}\text{C}$ , was calculated in a way similar to the work of *Kovaltsov et al.* [2012].

The number of simulated cascades was set to assure the statistical accuracy of the computed columnar isotope production to be better than 1%. It varied with the type of primaries and their initial energy, ranging from 1000 simulated cascades (for  $\alpha$ -particles with the energy of 100 GeV/nuc) to  $2 \cdot 10^7$  cascades (for 20 MeV protons).

Production functions computed in this way are tabulated in the Supporting information, for different isotopes and atmospheric depths. We emphasize that the computational results for  $\alpha$ -particles are given per nucleon but not per the entire  $\alpha$ -particle.

An example of the altitude (depth) profile of the production of  $^{36}\text{Cl}$  is shown in Fig. 1 for primary cosmic ray protons at several selected energies ranging from 0.1 GeV to 3 GeV. The total production is shown as solid lines with dots, while dashed curves depict contribution from secondary neutrons (the difference between the two is due to protons).

One can see that, for lower energy range (panel A), the production of  $^{36}\text{Cl}$  is dominated by direct spallation of atmospheric argon nuclei by primary protons in the upper atmospheric layer of a few tens of  $\text{g}/\text{cm}^2$ , while contribution of secondary particles is much smaller but becomes dominant at greater depths, where the cascade is fully developed. This is because low-energy primary particles have insufficient energy to initiate a developed nucleonic cascade. For energies of the primary particles greater than 1 GeV (panel B), the cascade is well developed and the production curve is smooth with nearly exponential attenuation with depth.

### 3. Cosmogenic isotope production

While the main result of this work, the altitude dependent yield functions, is discussed above, in this Section we present some applications and checks of the obtained results. A detailed recipe on how to compute the cosmogenic isotope production at a give time and location is given in Appendix.

#### 3.1. Columnar production

Columnar (viz. integrated within the entire atmospheric column) production of cosmogenic isotopes is often discussed [*Webber et al.*, 2007; *Kovaltsov et al.*, 2012]:

$$S_C = \int_0^H S(h) \cdot dh, \quad (6)$$

where  $H = 1033 \text{ g}/\text{cm}^2$  is the atmospheric depth at the mean sea level. Accordingly, we present here columnar productions for the purpose of comparison with earlier results (see Figures 2 through 6).

One can see that the columnar production curves computed here are in good agreement (within 5–10% for the energy above 100 MeV/nuc) with earlier results, except for one

case. While the present results for  $^{10}\text{Be}$  are fully consistent with those published earlier by *Kovaltsov and Usoskin* [2010] for energies above 100 MeV/nuc, the discrepancy with the results by *Webber et al.* [2007] is more systematic, by a factor of 1.5–1.7 (Figure 3a). We note that we used, for this isotope, the same cross-sections as *Webber and Higbie* [2003]. We have no clear explanation for this discrepancy, especially taking into account that the result for another beryllium isotope  $^7\text{Be}$  (Fig. 5a), which is very similar to  $^{10}\text{Be}$  in the sense of production, is in good agreement between the two models.

We note that the columnar production is shown only for illustration, while advanced studies should include also complex atmospheric transport which can be modelled only using the altitude profiles of the production functions  $S$ .

### 3.2. Global production rate

Also, for the purpose of illustration we depict the mean global production rate, due to GCR, of the five isotopes discussed here. The global production rate of an isotope is the averaged over the Globe columnar production rate, defined as

$$Q_G(t) = \frac{1}{4\pi} \int_{\Omega} \int_h Q(\phi(t), h, P_c(\Omega, t)) \cdot dh \cdot d\Omega, \quad (7)$$

where  $Q$  is given by Eq. 1, and integration is over the entire atmospheric column  $h$  (as in the columnar production) and over the Earth's surface (longitude and latitude)  $\Omega$ . The time dependence is included into variability of the modulation potential  $\phi$  and in the slow changes of the local geomagnetic cutoff rigidity  $P_c$  at each location.

The modulation potential  $\phi$  parameterizes the differential intensity of GCR in the vicinity of Earth,  $J(E, \phi(t))$  (see Eq. 1). It varies in accord with solar activity being low (higher GCR flux) and high (low GCR flux) around solar minima and maxima, respectively. The

formalism of the modulation potential approach is described in detail elsewhere [e.g., *Webber and Higbie*, 2003; *Vainio et al.*, 2009]. Here we use the modulation potential defined as in *Usoskin et al.* [2011] with the local interstellar spectrum (LIS), according to *Burger et al.* [2000]. We note that the exact value of  $\phi$  makes sense only for a fixed reference local interstellar spectrum of GCR [*Usoskin et al.*, 2005; *Herbst et al.*, 2010].

The large scale geomagnetic field provides additional shielding of the Earth from charged cosmic ray particles. The shielding is often parameterized in terms of the local effective geomagnetic rigidity cutoff  $P_c$  [*Cooke et al.*, 1991]. In the first approximation, the value of  $P_c$  at each location is determined by the geomagnetic latitude and the geomagnetic dipole moment  $M$ , which slowly varies on the centennial-millennial time scale in the range  $(6\text{--}12) \cdot 10^{22}$  A m<sup>2</sup> [e.g., *Genevey et al.*, 2008; *Nilsson et al.*, 2014].

The global production rates are shown in Figure 7 as a function of the modulation potential  $\phi$  for several values of the geomagnetic dipole moment  $M$ . It qualitatively resembles other similar plots shown earlier [e.g., *Masarik and Beer*, 1999; *Webber et al.*, 2007]. One can see that both parameters play an important role. The global production rates are also shown in Table 1 for the modern value of the geomagnetic dipole moment  $M = 7.8 \cdot 10^{22}$  A m<sup>2</sup>, for the cosmic ray modulation levels corresponding to the mean, minimum and maximum of solar cycles [*Usoskin et al.*, 2011].

We note different levels of the production rates for different isotopes: from  $< 10^{-4}$  for <sup>22</sup>Na to a few atoms per cm<sup>2</sup> per second for <sup>14</sup>C. This is defined by cross-sections of the processes (neutron capture for <sup>14</sup>C is much more likely than spallation reaction with a high energy threshold for other isotopes), and by abundance of the target atoms (argon,

which is the target for  $^{22}\text{Na}$ , is a factor  $\approx 100$  less abundant in the atmosphere than nitrogen and oxygen, which are targets for other elements).

Global production rates calculated here for  $^7\text{Be}$ ,  $^{10}\text{Be}$ ,  $^{14}\text{C}$  and  $^{22}\text{Na}$  are very close, within 5%, to those published by us earlier [*Usoskin and Kovaltsov*, 2008; *Kovaltsov and Usoskin*, 2010; *Kovaltsov et al.*, 2012; *Leppänen et al.*, 2012] using an older version of the CRAC model. Accordingly, comparisons with other simulation results and direct data that are discussed in great detail in those works, are valid also here. The only new for us isotope is  $^{36}\text{Cl}$ , whose global rate agrees within 15% with the value calculated by *Masarik and Beer* [2009].

We note that the mean global production makes sense only for  $^{14}\text{C}$ , which is globally mixed in the atmosphere. Recent direct in-situ measurements of stratospheric radiocarbon during 2002–2005 imply the global production of  $(2.2 \pm 0.6) \cdot 10^{26}$  atoms of  $^{14}\text{C}$  per year [*Kanu et al.*, 2016]. Our model (Fig.7a) predicts the global  $^{14}\text{C}$  production of  $2.36 \cdot 10^{26}$  atoms/yr for the period 2002–2005 (the mean  $\phi = 802$  MV [*Usoskin et al.*, 2011]), which is in good agreement with the measurements. Since the regional atmospheric transport and deposition prevents global mixing for other isotopes [*Beer et al.*, 2012] it makes little sense to consider the globally averaged production rate for them, especially for short-living ones such as  $^7\text{Be}$ .

For illustration, we show in Table 1 also (geomagnetically) polar and equatorial production rates of the isotopes, for the modern value of the geomagnetic dipole moment. One can see that the geomagnetic field shields cosmic rays effectively (equatorial production rates are about 15% of those in polar regions), while the solar cycle variability is strongest in polar regions (a factor two vs. 10–15% at the geomagnetic equator).

## 4. Testing the approach

In this Section we discuss some applications of the presented production functions for  $^{10}\text{Be}$  data in polar ice cores.

### 4.1. Solar cycle in $^{10}\text{Be}$

As an example of an application of the approach presented here, we have computed the deposition flux of  $^{10}\text{Be}$  in the northern polar region and compared it with the measurements in the NGRIP ice core [Berggren *et al.*, 2009]. The deposition flux was calculated in two steps. First, a 3D time varying pattern of the isotope atmospheric production was calculated using the yield functions presented here and applying the reconstruction of the modulation potential  $\phi$  based on data from the global neutron monitor network since 1951 [Usoskin *et al.*, 2011]. For the atmospheric transport we used a parameterization by Heikkilä *et al.* [2009, see Table 3 there], applying the mean latitudinal height profile of the tropopause. Finally, we calculated the deposition flux of  $^{10}\text{Be}$  in the Northern polar region. A 1-year delay due to the transport was applied. The calculated  $^{10}\text{Be}$  flux is in very good agreement with the real data, especially for the period 1951–1970 (see Figure 8). A minor (about 5%) discrepancy after 1970 is most likely related to the post-deposition effects in firn and/or to the regional climate variability on annual-decadal time scale [Pedro *et al.*, 2006, 2012]. The good agreement with data validates the yield-function for  $^{10}\text{Be}$ .

### 4.2. The period ca. 775 AD

The strongest known solar energetic particle (SEP) event took place in 775 AD [Miyake *et al.*, 2012; Usoskin *et al.*, 2013; Mekhaldi *et al.*, 2015]. Precise measurements of cosmogenic isotopes, in particular  $^{10}\text{Be}$  in ice cores, have been made for that particular period

[Miyake *et al.*, 2015; Sigl *et al.*, 2015; Mekhaldi *et al.*, 2015]. Not discussing the event itself, we compared the mean levels of the  $^{10}\text{Be}$  deposition flux for a few decades after the event with the prediction of our model. In Figure 9 we compare the modelled curves for  $^{10}\text{Be}$  deposition flux with that measured in four polar ice cores in Antarctica and Greenland (see Figure caption), averaged over the period 780–800 AD (the ice core dating corrections applied according to Sigl *et al.* [2015]), i.e. after the event and defined by GCR, not SEPs. These measured mean levels of the  $^{10}\text{Be}$  flux are shown by the horizontal hatched strip. The vertical hatched bar corresponds to the (cycle-averaged) value of the modulation potential for that period defined independently using the  $^{14}\text{C}$  record [Usoskin *et al.*, 2016]. The two black curves show the modelled deposition flux (production rate according to the present model and the atmospheric transport and deposition according to the parameterization by Heikkilä *et al.* [2009], the geomagnetic dipole moment  $M = 10^{23}$  A m<sup>2</sup> as reconstructed for that epoch by Licht *et al.* [2013]), for the northern and southern polar regions. One can see that the measured fluxes of  $^{10}\text{Be}$  are directly reproduced by the model within the possible uncertainties without any *ad hoc* adjustment or normalization which is typically applied to  $^{10}\text{Be}$  data.

Accordingly, we conclude that, with the new yield function we are able to quantitatively model the production of the cosmogenic radio-isotopes in the atmosphere.

## 5. Summary

We have performed a new consistent and precise computation of the production of five cosmogenic isotopes,  $^7\text{Be}$ ,  $^{10}\text{Be}$ ,  $^{14}\text{C}$ ,  $^{22}\text{Na}$  and  $^{36}\text{Cl}$ , in the Earth’s atmosphere by cosmic rays. Computations were made by means of a detailed Monte-Carlo simulation by the CRAC model using a recent version of the GEANT-4 tool. The results are presented in

the Supporting information in the form of tabulated yield (production) functions for a wide set of atmospheric depths. We provide, for the first time, a full detailed set of the altitude profiles of the production functions which makes it possible to apply the results directly as input for atmospheric transport models. Our results are in good agreement with most of the earlier published works for columnar and global isotopic production rates. Comparison of the computations with measured data of  $^{10}\text{Be}$  for the last decades and also for a period around 780 AD validates the approach also in quantitative terms.

### Appendix: Recipe for computation of the cosmogenic isotope production

Here we present a recipe on how to compute the production rate  $Q(h, P_c, t)$  of a cosmogenic isotope at a given location and time. The location is defined by the atmospheric depth  $h$  and the local geomagnetic rigidity cutoff  $P_c$ .

First, the yield function for a cosmic ray specie  $i$  (proton or  $\alpha$ -particle) should be computed for the given atmospheric depth as  $Y_i(h, E) = \pi \cdot S_i(h, E)$  (see Eq. 3), where  $S_i(h, E)$  is taken from an appropriate table in the Supporting information. Note that the energy of  $\alpha$ -particles should be taken as kinetic energy per nucleon. Next, the production rate of the isotope should be computed using Equation 1, where the cutoff energy is calculated from the local geomagnetic rigidity cutoff  $P_c$  using formula 2. For numerical integration, values of  $Y$  can be interpolated by a power-law function between the tabulated points. The value of  $P_c$  as well as spectra  $J_i$  of cosmic-ray protons and  $\alpha$ -particles should be known independently. For the spectra we recommend using the force-field approximation where spectra are parameterized via a single parameter, the modulation potential  $\phi$  (see detail in *Usoskin et al. [2005]*). Values for the modulation potential are given, e.g., by *Usoskin et al. [2011]* and updated at <http://cosmicrays.oulu.fi/phi/phi.html>.



**Acknowledgments.** This work was supported by the Center of Excellence ReSoLVE (project No. 272157). Supporting data are included as tables in the SI file; any additional data may be obtained from IGU (email: ilya.usoskin@oulu.fi).

## References

- Agostinelli, S., et al. (2003), Geant4 a simulation toolkit, *Nuclear Instruments and Methods in Physics Research Section A: Accelerators, Spectrometers, Detectors and Associated Equipment*, 506(3), 250 – 303, doi:http://dx.doi.org/10.1016/S0168-9002(03)01368-8.
- Allison, J., et al. (2006), Geant4 developments and applications, *Nuclear Science, IEEE Transactions on*, 53(1), 270–278, doi:10.1109/TNS.2006.869826.
- Beer, J., K. McCracken, and R. von Steiger (2012), *Cosmogenic Radionuclides: Theory and Applications in the Terrestrial and Space Environments*, Springer, Berlin.
- Berggren, A.-M., J. Beer, G. Possnert, A. Aldahan, P. Kubik, M. Christl, S. J. Johnsen, J. Abreu, and B. M. Vinther (2009), A 600-year annual  $^{10}\text{Be}$  record from the NGRIP ice core, Greenland, *Geophys. Res. Lett.*, 36, L11801.
- Burger, R., M. Potgieter, and B. Heber (2000), Rigidity dependence of cosmic ray proton latitudinal gradients measured by the ulysses spacecraft: Implications for the diffusion tensor, *J. Geophys. Res.*, 105, 27,447–27,456.
- Cooke, D., J. Humble, M. Shea, D. Smart, N. Lund, I. Rasmussen, B. Byrnek, P. Goret, and N. Petrou (1991), On cosmic-ray cut-off terminology., *Nuovo Cimento C*, 14, 213–234.

- Delaygue, G., S. Bekki, and E. Bard (2015), Modelling the stratospheric budget of beryllium isotopes, *TELLUS SERIES B-CHEMICAL AND PHYSICAL METEOROLOGY*, *67*, 28,582, doi:10.3402/tellusb.v67.28582.
- Desorgher, L., K. Kudela, E. Flueckiger, R. Buetikofer, M. Storini, and V. Kalegaev (2009), Comparison of Earth’s magnetospheric magnetic field models in the context of cosmic ray physics, *Acta Geophys.*, *57*(1), 75–87, doi:10.2478/s11600-008-0065-3.
- Dorman, L. (2004), *Cosmic Rays in the Earth’s Atmosphere and Underground*, Kluwer Academic Publishers, Dordrecht.
- Fassò, A., A. Ferrari, J. Ranft, and P. Sala (2001), Fluka: Status and prospective of hadronic applications, in *Proc. Monte Carlo 2000 Conf.*, edited by A. K. et al., pp. 955–960, Springer, Berlin.
- Field, C., G. Schmidt, D. Koch, and C. Salyk (2006), Modeling production and climate-related impacts on  $^{10}\text{Be}$  concentration in ice cores, *J. Geophys. Res.*, *111*, D15,107.
- GEANT4 collaboration (2013), *Physics reference manual (version geant4 10.0)*, available from <http://geant4.cern.ch/support/userdocuments.shtml>.
- Genevey, A., Y. Gallet, C. G. Constable, M. Korte, and G. Hulot (2008), ArcheoInt: An upgraded compilation of geomagnetic field intensity data for the past ten millennia and its application to the recovery of the past dipole moment, *Geochem., Geophys., Geosyst.*, *9*, Q04038, doi:10.1029/2007GC001881.
- Grieder, P. (2001), *Cosmic Rays at Earth*, Elsevier Science, Amsterdam.
- Heck, D., J. Knapp, J. Capdevielle, G. Schatz, and T. Thouw (1998), Corsika: A monte carlo code to simulate extensive air showers, in *FZKA 6019*, Forschungszentrum, Karlsruhe.

- Heikkilä, U., J. Beer, and J. Feichter (2009), Meridional transport and deposition of atmospheric  $^{10}\text{Be}$ , *Atmos. Chem. Phys.*, *9*, 515–527.
- Herbst, K., A. Kopp, B. Heber, F. Steinhilber, H. Fichtner, K. Scherer, and D. Matthiä (2010), On the importance of the local interstellar spectrum for the solar modulation parameter, *J. Geophys. Res.*, *115*, D00I20, doi:10.1029/2009JD012557.
- Inceoglu, F., R. Simoniello, V. F. Knudsen, C. Karoff, J. Olsen, S. Turck-Chiéze, and B. H. Jacobsen (2015), Grand solar minima and maxima deduced from  $^{10}\text{be}$  and  $^{14}\text{c}$ : magnetic dynamo configuration and polarity reversal, *Astron. Astrophys.*, *577*, A20.
- Ioannidou, A., and J. Paatero (2014), Activity size distribution and residence time of  $^7\text{Be}$  aerosols in the Arctic atmosphere, *Atmos. Env.*, *88*, 99–106, doi:10.1016/j.atmosenv.2013.12.046.
- Jöckel, P., M. G. Lawrence, and C. A. M. Brenninkmeijer (1999), Simulations of cosmogenic  $^{14}\text{CO}$  using the three-dimensional atmospheric model MATCH: Effects of  $^{14}\text{C}$  production distribution and the solar cycle, *J. Geophys. Res.*, *104*, 11, doi:10.1029/1999JD900061.
- Jöckel, P., C. A. M. Brenninkmeijer, M. G. Lawrence, and P. Siegmund (2003), The detection of solar proton produced  $^{14}\text{CO}$ , *Atmos. Chem. Phys.*, *3*, 999–1005.
- Jordan, C. E., J. E. Dibb, and R. C. Finkel (2003),  $^{10}\text{Be}/^7\text{Be}$  tracer of atmospheric transport and stratosphere-troposphere exchange, *J. Geophys. Res.*, *108*, 4234, doi:10.1029/2002JD002395.
- Jull, A., S. Cloudt, D. Donahue, J. Sisterson, R. Reedy, and J. Masarik (1998),  $^{14}\text{c}$  depth profiles in apollo 15 and 17 cores and lunar rock 68815, *Geochimica et Cosmochimica Acta*, *62*, 3025–3036, doi:10.1016/S0016-7037(98)00193-8.

- Kanu, A. M., L. L. Comfort, T. P. Guilderson, P. J. Cameron-Smith, D. J. Bergmann, E. L. Atlas, S. Schauffler, and K. A. Boering (2016), Measurements and modeling of contemporary radiocarbon in the stratosphere, *Geophys. Res. Lett.*, *43*(3), 1399–1406, doi:10.1002/2015GL066921, 2015GL066921.
- Kovaltsov, G., and I. Usoskin (2010), A new 3D numerical model of cosmogenic nuclide  $^{10}\text{Be}$  production in the atmosphere, *Earth Planet.Sci.Lett.*, *291*, 182–188.
- Kovaltsov, G., A. Mishev, and I. Usoskin (2012), A new model of cosmogenic production of radiocarbon  $^{14}\text{C}$  in the atmosphere, *Earth Planet. Sci. Lett.*, *337*, 114–120.
- Lal, D., and B. Peters (1962), Cosmic ray produced isotopes and their application to problems in geophysics,, in *Progress in Elementary Particle and Cosmic Ray Physics*,, vol. 6, edited by J. Wilson and S. Wouthuysen, pp. 77–243, North Holland, Amsterdam.
- Lange, H., et al. (1995), Production of residual nuclei by alpha-induced reactions on C, N, O, Mg, Al and Si up to 170 MeV, *Appl. Rad. Isot.*, *46*(2), 93–112, doi:10.1016/0969-8043(94)00124-I.
- Leppänen, A.-P., I. G. Usoskin, G. A. Kovaltsov, and J. Paatero (2012), Cosmogenic  $^7\text{Be}$  and  $^{22}\text{Na}$  in Finland: Production, observed periodicities and the connection to climatic phenomena, *J. Atmos. Solar-Terr. Phys.*, *74*, 164–180, doi:10.1016/j.jastp.2011.10.017.
- Licht, A., G. Hulot, Y. Gallet, and E. Thébaudt (2013), Ensembles of low degree archeo-magnetic field models for the past three millennia, *Phys. Earth Planet. Inter.*, *224*, 38–67, doi:10.1016/j.pepi.2013.08.007.
- Lingenfelter, R. (1963), Production of carbon 14 by cosmic-ray neutrons, *Rev. Geophys. Space Phys.*, *1*, 35–55.

- Lingenfelter, R., and R. Ramaty (1970), Astrophysical and geophysical variations in  $c-14$  production, in *Proc. 12th Nobel symposium, Radiocarbon variations and absolute chronology*, edited by I. Olsson, pp. 513–537, John Wiley & Sons, NY.
- Masarik, J., and J. Beer (1999), Simulation of particle fluxes and cosmogenic nuclide production in the earth’s atmosphere., *J. Geophys. Res.*, *104*, 12,099–12,111.
- Masarik, J., and J. Beer (2009), An updated simulation of particle fluxes and cosmogenic nuclide production in the Earth’s atmosphere, *J. Geophys. Res.*, *114*, D11,103, doi:10.1029/2008JD010557.
- McCracken, K. (2004), Geomagnetic and atmospheric effects upon the cosmogenic  $^{10}\text{be}$  observed in polar ice, *J. Geophys. Res.*, *109*(A18), doi:10.1029/2003JA010060.
- McCracken, K., F. McDonald, J. Beer, G. Raisbeck, and F. Yiou (2004), A phenomenological study of the long-term cosmic ray modulation, 850-1958 ad, *J. Geophys. Res.*, *109*(A18), 12,103, doi:10.1029/2004JA010685.
- Mekhaldi, F., et al. (2015), Multiradionuclide evidence for the solar origin of the cosmic-ray events of AD 774/5 and 993/4, *Nature Comm.*, *6*, 8611, doi:10.1038/ncomms9611.
- Miyake, F., K. Nagaya, K. Masuda, and T. Nakamura (2012), A signature of cosmic-ray increase in ad 774-775 from tree rings in Japan, *Nature*, *486*, 240–242, doi:10.1038/nature11123.
- Miyake, F., A. Suzuki, K. Masuda, K. Horiuchi, H. Motoyama, H. Matsuzaki, Y. Motizuki, K. Takahashi, and Y. Nakai (2015), Cosmic ray event of A.D. 774-775 shown in quasi-annual  $^{10}\text{Be}$  data from the Antarctic Dome Fuji ice core, *Geophys. Res. Lett.*, *42*, 84–89, doi:10.1002/2014GL062218.

- Muscheler, R., F. Joos, J. Beer, S. Müller, M. Vonmoos, and I. Snowball (2007), Solar activity during the last 1000 yr inferred from radionuclide records, *Quater. Sci. Rev.*, *26*, 82–97, doi:10.1016/j.quascirev.2006.07.012.
- Nilsson, A., R. Holme, M. Korte, N. Suttie, and M. Hill (2014), Reconstructing Holocene geomagnetic field variation: new methods, models and implications, *Geophys. J. Int.*, *198*, 229–248, doi:10.1093/gji/ggu120.
- O’Brien, K. (1979), Secular variations in the production of cosmogenic isotopes in the earth’s atmosphere, *J. Geophys. Res.*, *84*, 423–431.
- Pacini, A. A., I. G. Usoskin, K. Mursula, E. Echer, and H. Evangelista (2015), Signature of a sudden stratospheric warming in the near-ground  $^7\text{Be}$  flux, *Atmos. Env.*, *113*, 27–31, doi:10.1016/j.atmosenv.2015.04.065.
- Pedro, J., T. van Ommen, M. Curran, V. Morgan, A. Smith, and A. McMorrow (2006), Evidence for climate modulation of the  $^{10}\text{Be}$  solar activity proxy, *J. Geophys. Res.*, *111*, D21105, doi:10.1029/2005JD006764.
- Pedro, J. B., J. R. McConnell, T. D. van Ommen, D. Fink, M. A. J. Curran, A. M. Smith, K. J. Simon, A. D. Moy, and S. B. Das (2012), Solar and climate influences on ice core  $^{10}\text{Be}$  records from Antarctica and Greenland during the neutron monitor era, *Earth Planet. Sci. Lett.*, *355*, 174–186, doi:10.1016/j.epsl.2012.08.038.
- Picone, J. M., A. E. Hedin, D. P. Drob, and A. C. Aikin (2002), NRLMSISE-00 empirical model of the atmosphere: Statistical comparisons and scientific issues, *J. Geophys. Res.*, *107*, 1468, doi:10.1029/2002JA009430.
- Reyss, J.-L., Y. Yokoyama, and F. Guichard (1981), Production cross sections of Al-26, Na-22, Be-7 from argon and of Be-10, Be-7 from nitrogen – Implications for production

- rates of Al-26 and Be-10 in the atmosphere, *Earth Planet. Sci. Lett.*, *53*, 203–210, doi:10.1016/0012-821X(81)90154-0.
- Sakaguchi, A., Y. Ohtsuka, K.-i. Yokota, K. Sasaki, K. Komura, and M. Yamamoto (2005), Cosmogenic radionuclide  $^{22}\text{Na}$  in the Lake Biwa system (Japan): residence time, transport and application to the hydrology, *Earth Planet. Sci. Lett.*, *231*, 307–316, doi:10.1016/j.epsl.2004.12.023.
- Sigl, M., et al. (2015), Timing and climate forcing of volcanic eruptions for the past 2,500 years, *Nature*, *523*, 543–549, doi:10.1038/nature14565.
- Solanki, S., I. Usoskin, B. Kromer, M. Schüssler, and J. Beer (2004), Unusual activity of the sun during recent decades compared to the previous 11,000 years, *Nature*, *431*, 1084–1087, doi:10.1038/nature02995.
- Steinhilber, F., et al. (2012), 9,400 years of cosmic radiation and solar activity from ice cores and tree rings, *Proc. Nat. Acad. Sci. USA*, *109*(16), 5967–5971, doi:10.1073/pnas.1118965109.
- Tatischeff, V., B. Kozlovsky, J. Kiener, and R. J. Murphy (2006), Delayed X- and Gamma-Ray Line Emission from Solar Flare Radioactivity, *Astrophys. J. Suppl.*, *165*, 606–617, doi:10.1086/505112.
- Usoskin, I., and G. Kovaltsov (2008), Production of cosmogenic  $^7\text{Be}$  isotope in the atmosphere: Full 3D modelling, *J. Geophys. Res.*, *113*, "D12,107", doi:10.1029/2007JD009725.
- Usoskin, I., S. Solanki, G. Kovaltsov, J. Beer, and B. Kromer (2006), Solar proton events in cosmogenic isotope data, *Geophys. Res. Lett.*, *33*, L08,107, doi:10.1029/2006GL026059.

- Usoskin, I. G. (2013), A History of Solar Activity over Millennia, *Living Rev. Solar Phys.*, *10*, 1, doi:10.12942/lrsp-2013-1.
- Usoskin, I. G., K. Alanko-Huotari, G. A. Kovaltsov, and K. Mursula (2005), Heliospheric modulation of cosmic rays: Monthly reconstruction for 1951–2004, *J. Geophys. Res.*, *110*, A12108, doi:10.1029/2005JA011250.
- Usoskin, I. G., G. A. Bazilevskaya, and G. A. Kovaltsov (2011), Solar modulation parameter for cosmic rays since 1936 reconstructed from ground-based neutron monitors and ionization chambers, *J. Geophys. Res.*, *116*, A02104, doi:10.1029/2010JA016105.
- Usoskin, I. G., B. Kromer, F. Ludlow, J. Beer, M. Friedrich, G. A. Kovaltsov, S. K. Solanki, and L. Wacker (2013), The AD775 cosmic event revisited: the Sun is to blame, *Astron. Astrophys.*, *552*, L3, doi:10.1051/0004-6361/201321080.
- Usoskin, I. G., G. Hulot, Y. Gallet, R. Roth, A. Licht, F. Joos, G. A. Kovaltsov, E. Thébault, and A. Khokhlov (2014), Evidence for distinct modes of solar activity, *Astron. Astrophys.*, *562*, L10, doi:10.1051/0004-6361/201423391.
- Usoskin, I. G., Y. Gallet, F. Lopes, G. A. Kovaltsov, and G. Hulot (2016), Solar activity during the Holocene: the Hallstatt cycle and its consequence for grand minima and maxim, *Astron. Astrophys.*, *587*, A150, doi:10.1051/0004-6361/201527295.
- Vainio, R., et al. (2009), Dynamics of the Earth’s particle radiation environment, *Space Sci. Rev.*, *147*, 187–231, doi:10.1007/s11214-009-9496-7.
- Vonmoos, M., J. Beer, and R. Muscheler (2006), Large variations in holocene solar activity: Constraints from  $^{10}\text{be}$  in the greenland ice core project ice core, *J. Geophys. Res.*, *111*(A10), A10,105, doi:10.1029/2005JA011500.



Webber, W., and P. Higbie (2003), Production of cosmogenic be nuclei in the earth's atmosphere by cosmic rays: Its dependence on solar modulation and the interstellar cosmic ray spectrum, *J. Geophys. Res.*, *108*, 1355, doi:10.1029/2003JA009863.

Webber, W., P. Higbie, and K. McCracken (2007), Production of the cosmogenic isotopes  $^3\text{h}$ ,  $^7\text{be}$ ,  $^{10}\text{be}$ , and  $^{36}\text{cl}$  in the earth's atmosphere by solar and galactic cosmic rays, *J. Geophys. Res.*, *112*, doi:10.1029/2007JA012499.

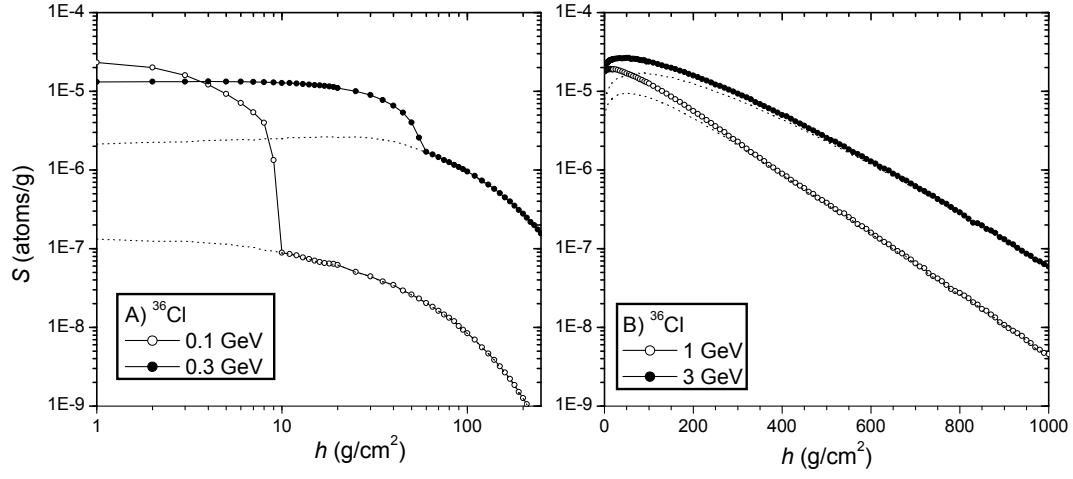


**Figure 1.** Production functions  $S$  (see Equation 5) of  $^{36}\text{Cl}$  by protons of given energy (as denoted in the legends) as a function of the atmospheric depth. Dotted lines depict contribution from secondary neutrons.

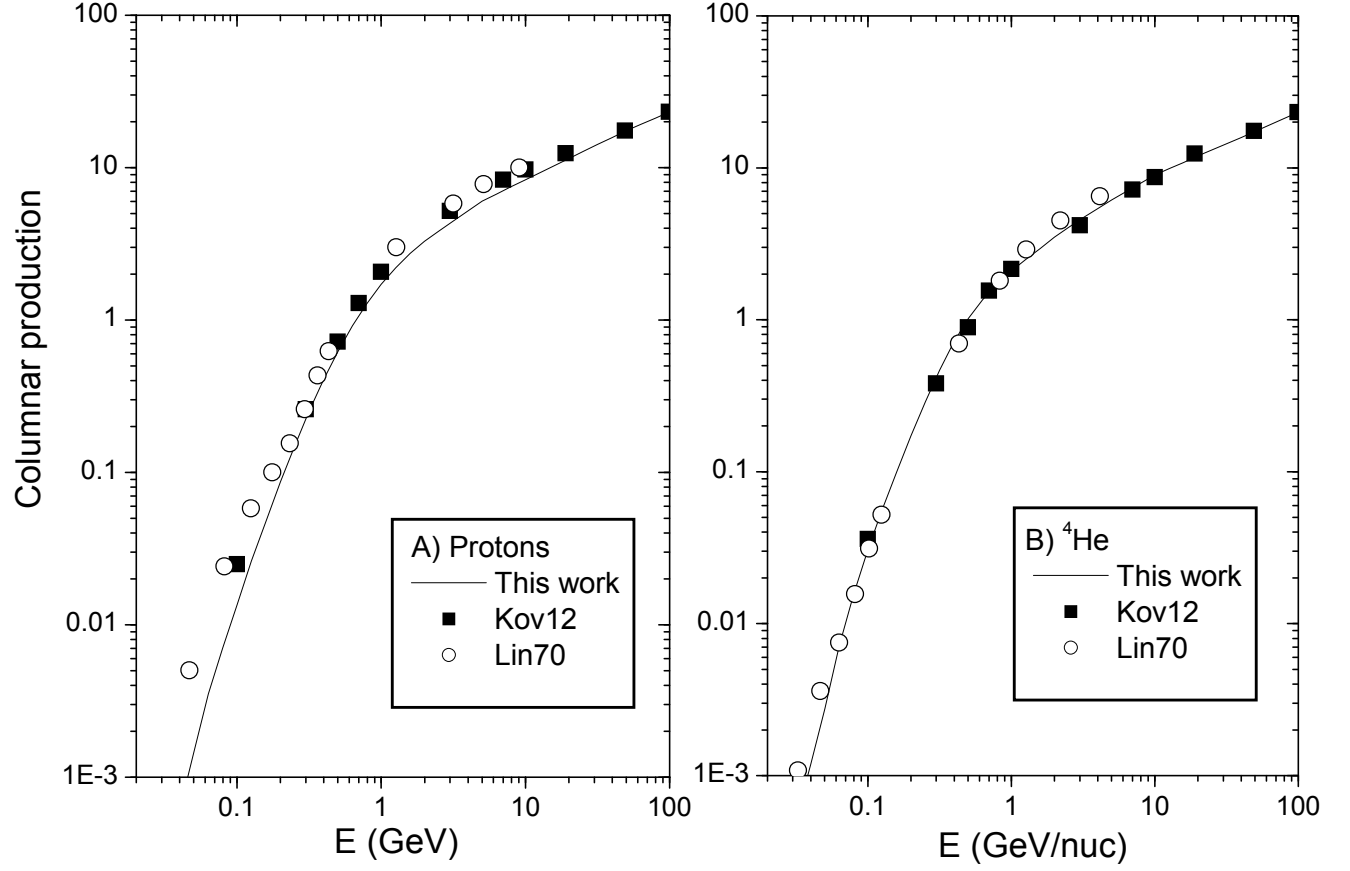


**Figure 2.** Columnar production  $S_C$  (atoms per incident nucleon) of the cosmogenic isotope  $^{14}\text{C}$  by protons (panel A) and  $\alpha$ -particles (panel B). The black line depicts the results of this work, black squares (Kov12) and open circles (Lin70) represent the results by *Kovaltsov et al.* [2012] and *Lingenfelter and Ramaty* [1970], respectively.

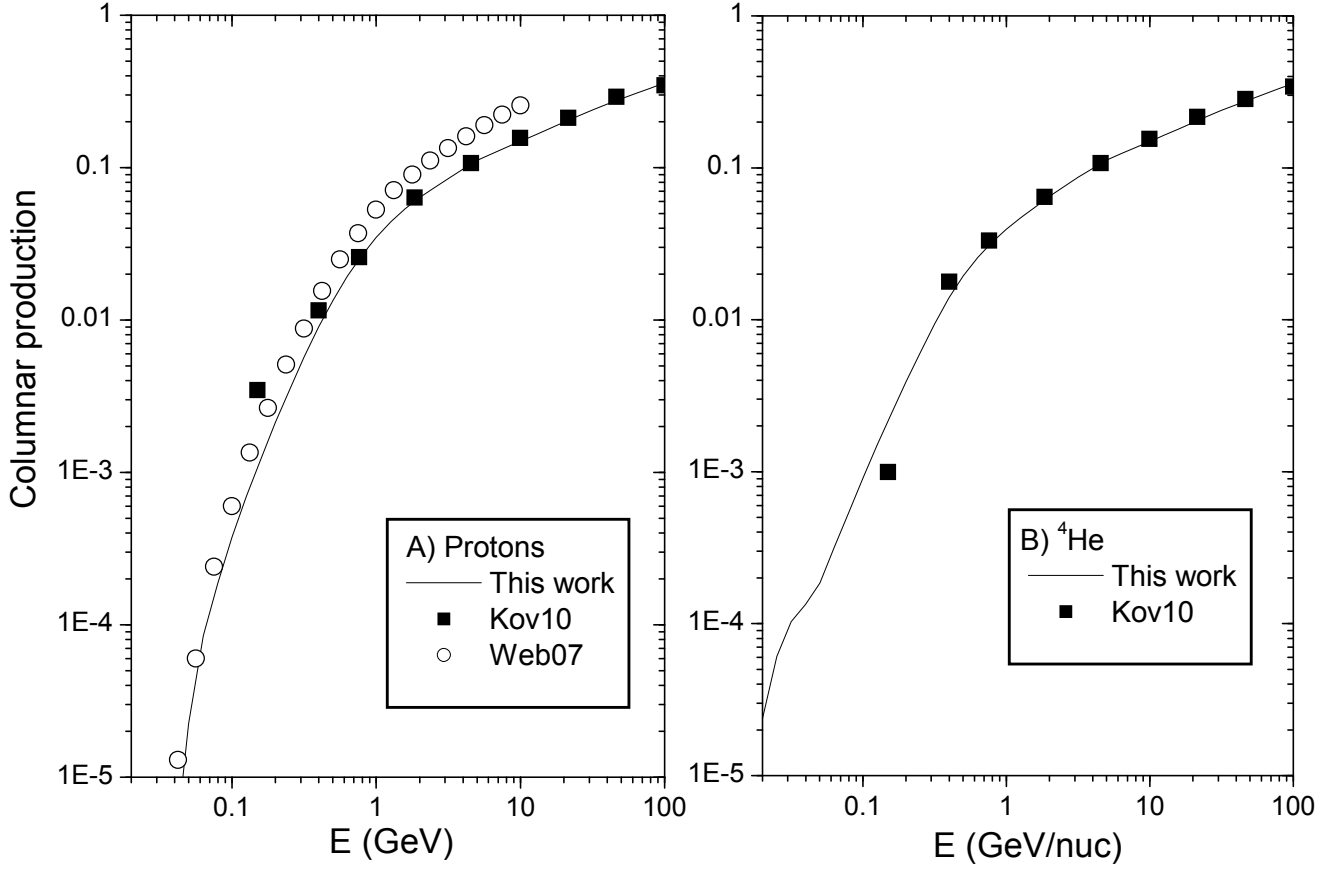


**Figure 3.** Columnar production  $S_C$  (atoms per incident nucleon) of the cosmogenic isotope  $^{10}\text{Be}$  by protons (panel A) and  $\alpha$ -particles (panel B). The black lines depict the results of this work, black squares (Kov10) and open circles (Web07) represent the results by *Kovaltsov and Usoskin* [2010] and *Webber et al.* [2007], respectively.

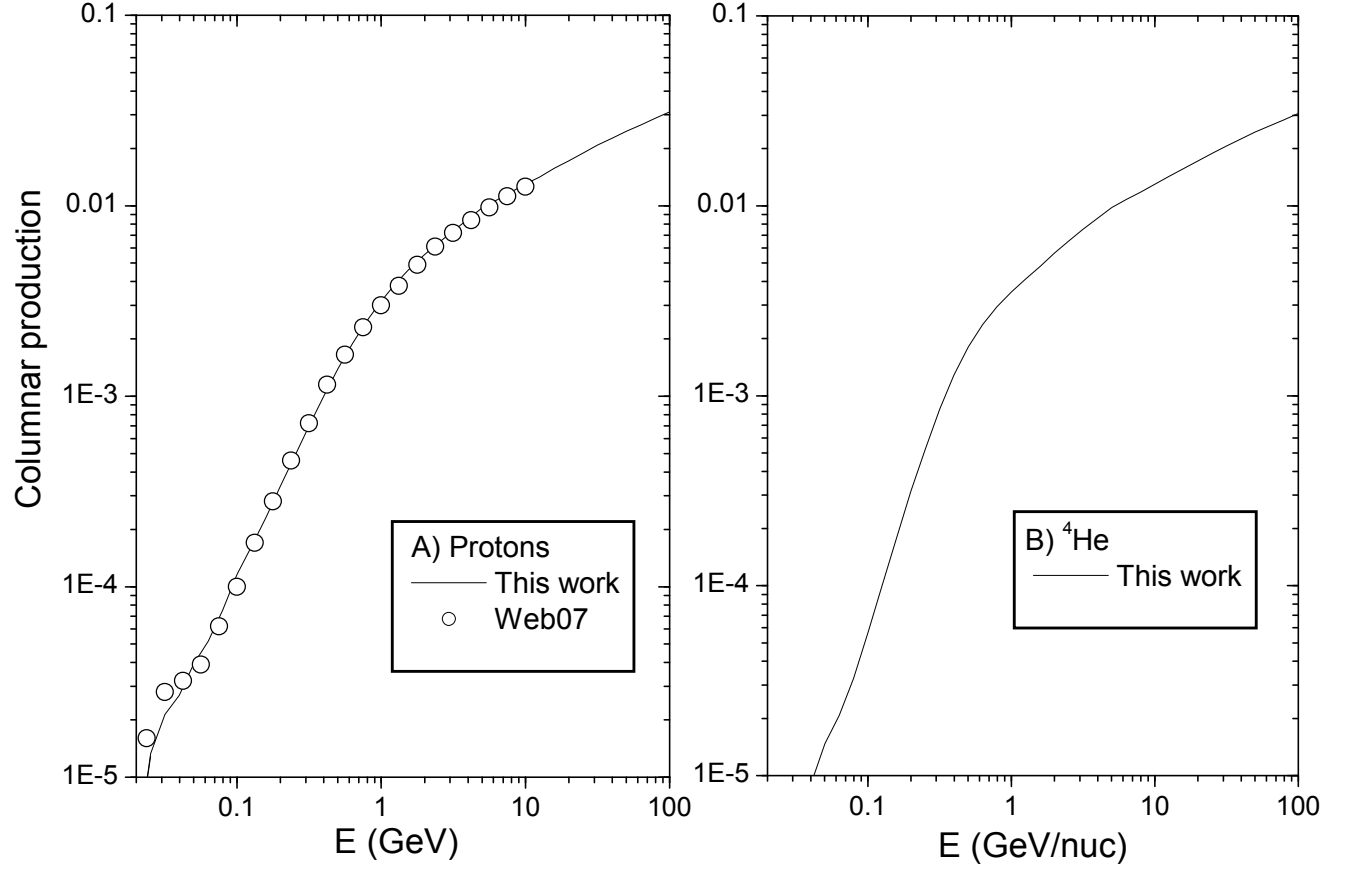


**Figure 4.** Columnar production  $S_C$  (atoms per incident nucleon) of the cosmogenic isotope  $^{36}\text{Cl}$  by protons (panel A) and  $\alpha$ -particles (panel B). The black lines depict the results of this work, while open circles (Web07) represent the results by *Webber et al.* [2007].

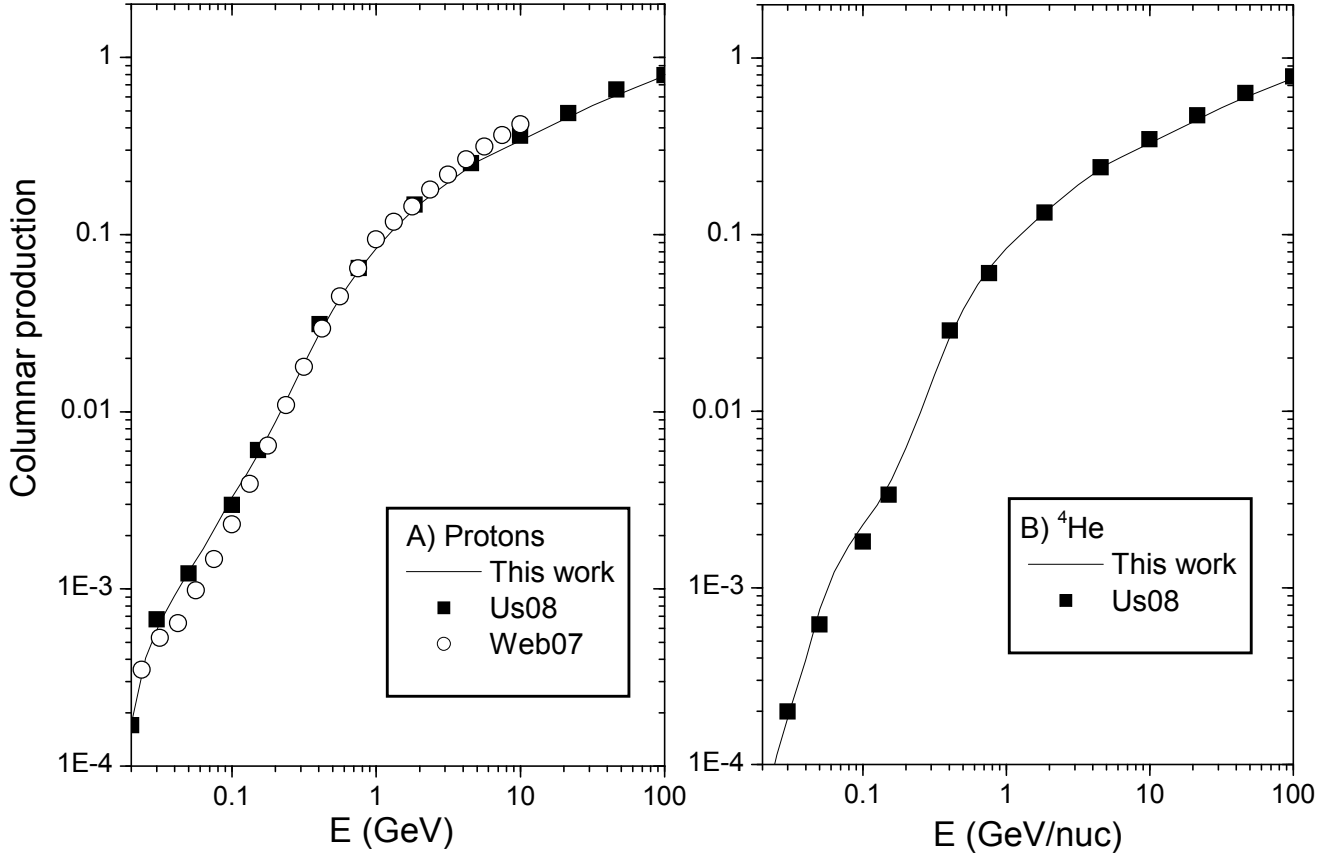


**Figure 5.** Columnar production  $S_C$  (atoms per incident nucleon) of the cosmogenic isotope  $^7\text{Be}$  by protons (panel A) and  $\alpha$ -particles (panel B). The black lines depict the results of this work, black squares (Us08) and open circles (Web07) represent the results by *Usoskin and Kovaltsov* [2008] and *Webber et al.* [2007], respectively.

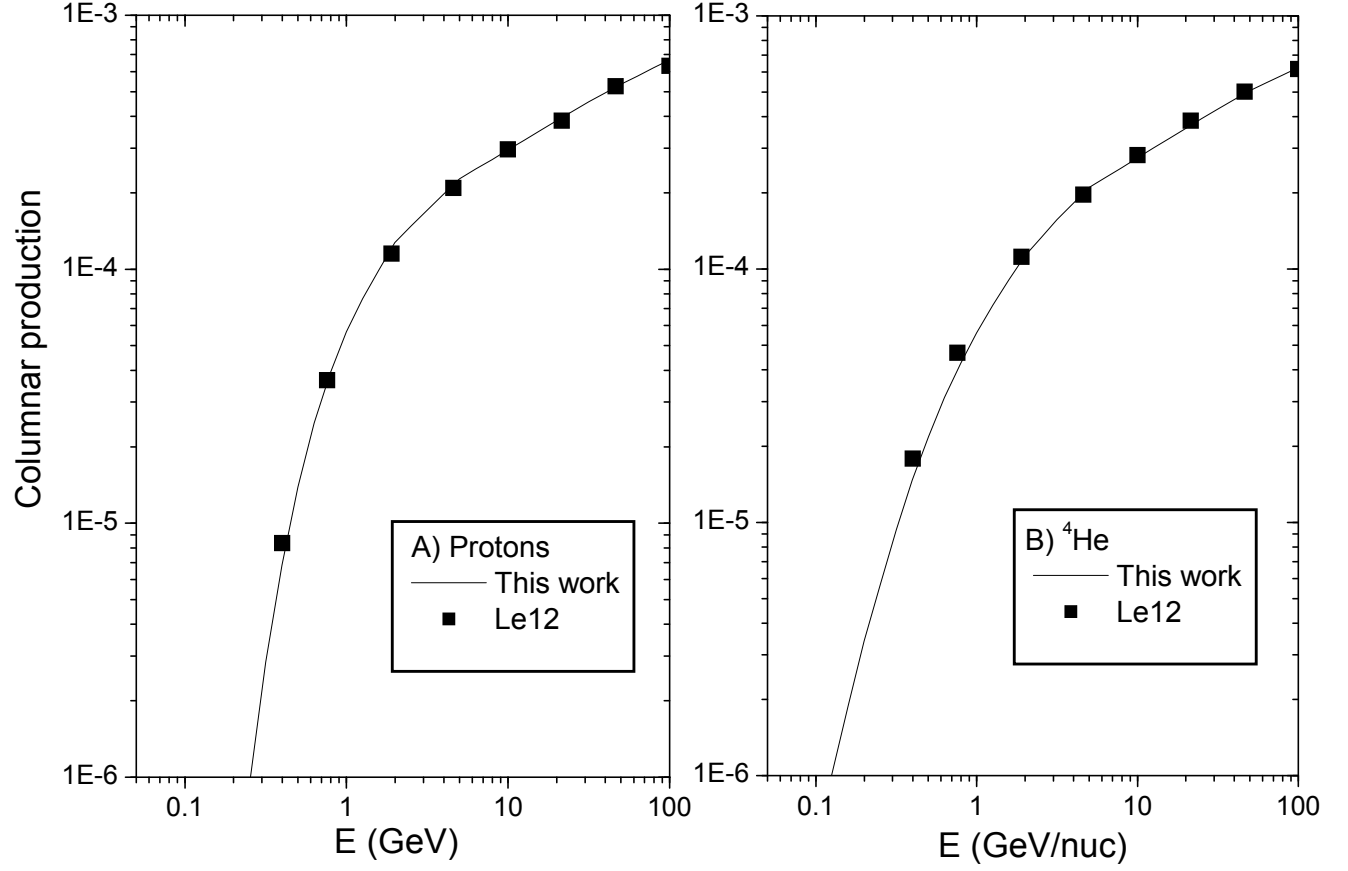


**Figure 6.** Columnar production  $S_C$  (atoms per incident nucleon) of the cosmogenic isotope  $^{22}\text{Na}$  by protons (panel A) and  $\alpha$ -particles (panel B). The black lines depict the results of this work, while black squares (Le12) represent the results by *Leppänen et al.* [2012].

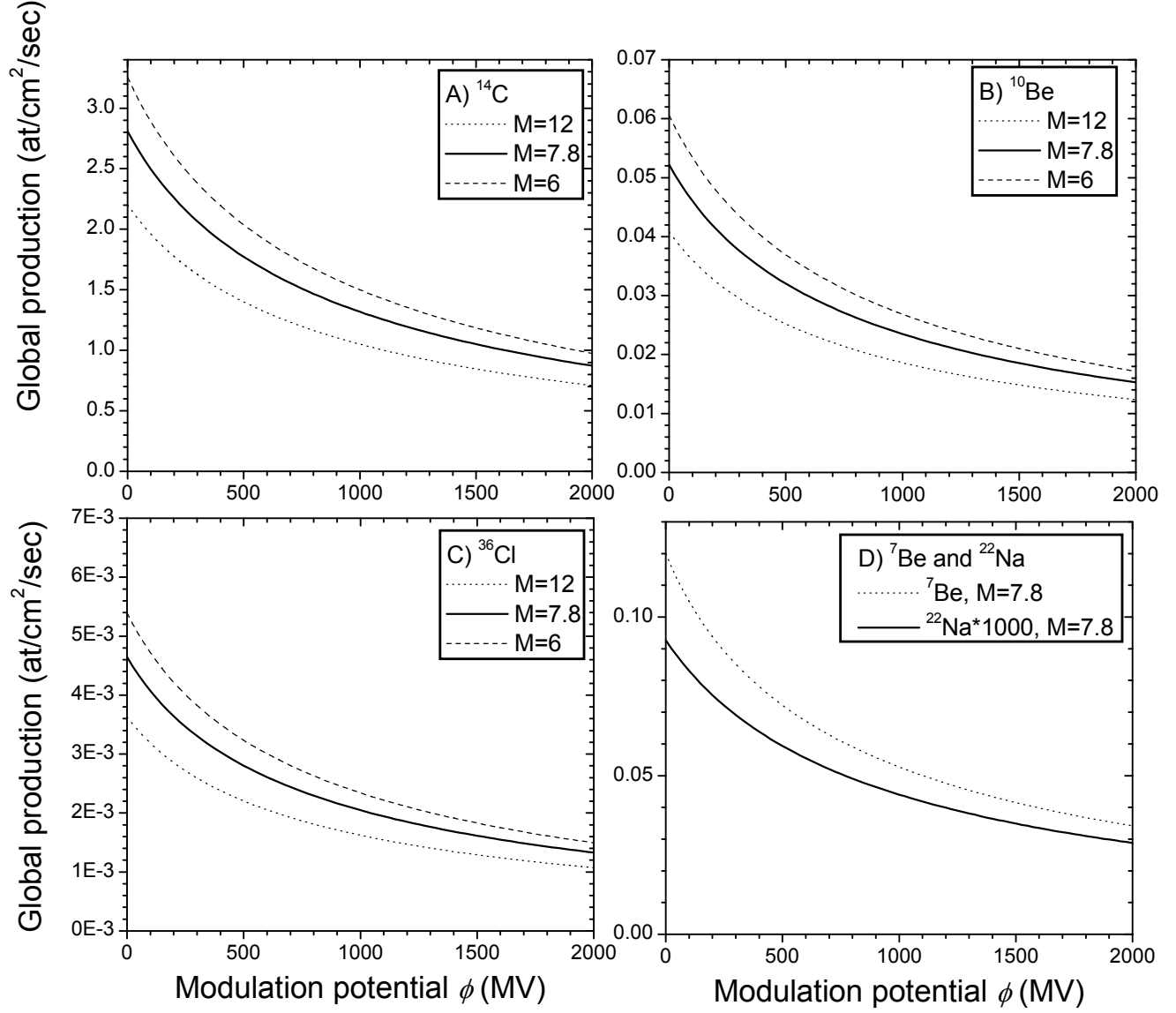


**Figure 7.** Global production rates of cosmogenic isotopes as a function of the modulation potential  $\phi$ , for different values of the geomagnetic dipole moment  $M$  (in  $10^{22}$  A m<sup>2</sup>), as denoted in the legends. Panels A through D correspond to isotopes  $^{14}\text{C}$ ,  $^{10}\text{Be}$ ,  $^{36}\text{Cl}$ ,  $^7\text{Be}$  and  $^{22}\text{Na}$  (scaled up by a factor 1000), respectively.



**Table 1.** Global, polar (geomagnetic pole) and equatorial (geomagnetic equator) production rates of the five cosmogenic radio-isotopes for the modern conditions (the geomagnetic dipole moment  $M = 7.8 \cdot 10^{23}$  A m<sup>2</sup>), for the mean, minimum and maximum modulation potentials:  $\langle \phi \rangle = 650$ ,  $\phi_{\min} = 300$  and  $\phi_{\max} = 1200$  MV, respectively. The production rates are given in atoms/cm<sup>2</sup>/sec.

Isotope	Global production			Polar production			Equatorial production		
	mean	minimum	maximum	mean	minimum	maximum	mean	minimum	maximum
<sup>7</sup> Be	$6.5 \cdot 10^{-2}$	$8.5 \cdot 10^{-2}$	$4.8 \cdot 10^{-2}$	$1.45 \cdot 10^{-1}$	$2.2 \cdot 10^{-1}$	$9.1 \cdot 10^{-2}$	$2.1 \cdot 10^{-2}$	$2.3 \cdot 10^{-2}$	$1.9 \cdot 10^{-2}$
<sup>10</sup> Be	$2.9 \cdot 10^{-2}$	$3.8 \cdot 10^{-2}$	$2.1 \cdot 10^{-2}$	$6.4 \cdot 10^{-2}$	$9.5 \cdot 10^{-2}$	$4.0 \cdot 10^{-2}$	$9.6 \cdot 10^{-3}$	$1.0 \cdot 10^{-2}$	$8.7 \cdot 10^{-3}$
<sup>14</sup> C	1.6	2.07	1.2	3.42	5.02	2.21	$5.7 \cdot 10^{-1}$	$6.1 \cdot 10^{-1}$	$5.2 \cdot 10^{-1}$
<sup>22</sup> Na	$5.4 \cdot 10^{-5}$	$6.9 \cdot 10^{-5}$	$4.0 \cdot 10^{-5}$	$1.15 \cdot 10^{-4}$	$1.7 \cdot 10^{-4}$	$7.5 \cdot 10^{-5}$	$1.8 \cdot 10^{-5}$	$1.9 \cdot 10^{-5}$	$1.6 \cdot 10^{-5}$
<sup>36</sup> Cl	$2.5 \cdot 10^{-3}$	$3.3 \cdot 10^{-3}$	$1.85 \cdot 10^{-3}$	$5.6 \cdot 10^{-3}$	$8.5 \cdot 10^{-3}$	$3.5 \cdot 10^{-3}$	$8.3 \cdot 10^{-4}$	$8.8 \cdot 10^{-4}$	$7.5 \cdot 10^{-4}$

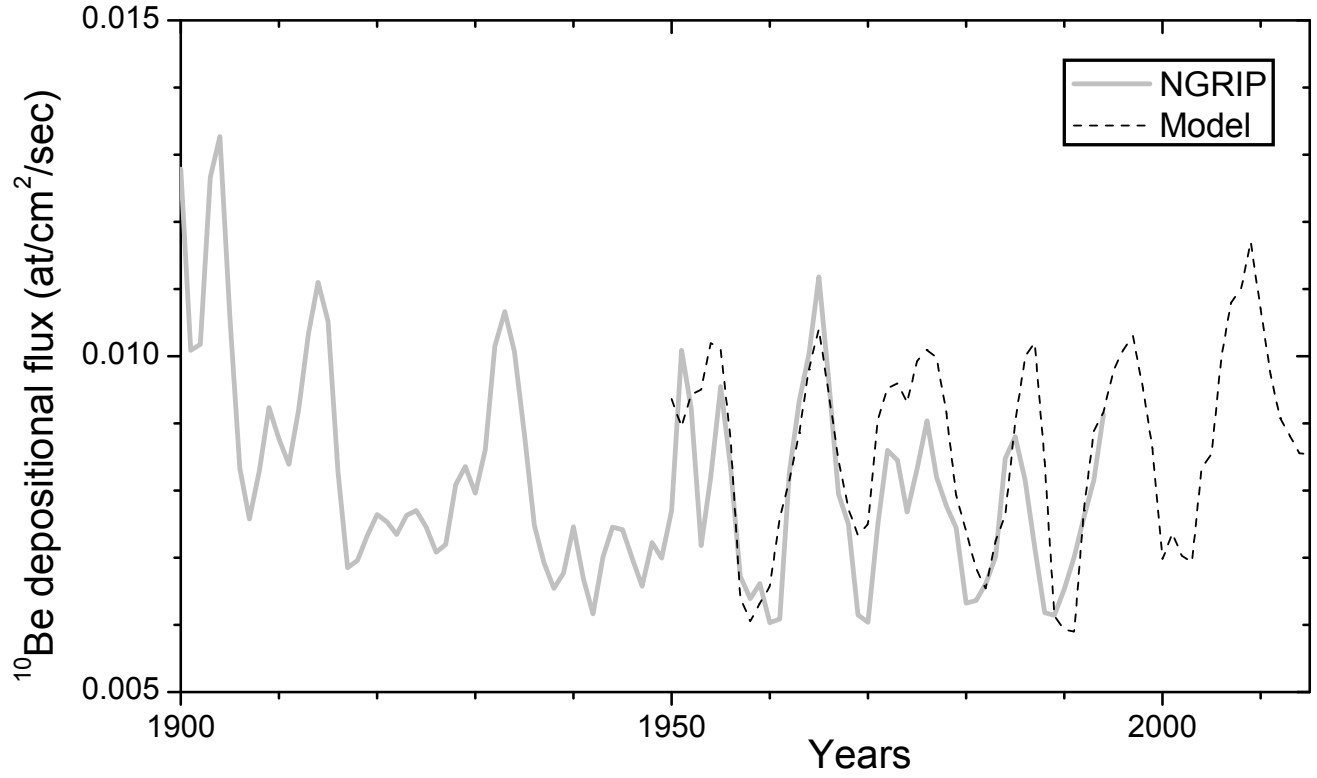


**Figure 8.** Annual deposition flux of  $^{10}\text{Be}$  in polar regions computed using the present production model (atmospheric transport was parameterized according to *Heikkilä et al.* [2009]) for the last decades. The grey curve depicts the measured series from the Greenland NGRIP ice core [*Berggren et al.*, 2009], while the dashed black curve is the model result. The data are smoothed with the 1-2-1 filter.

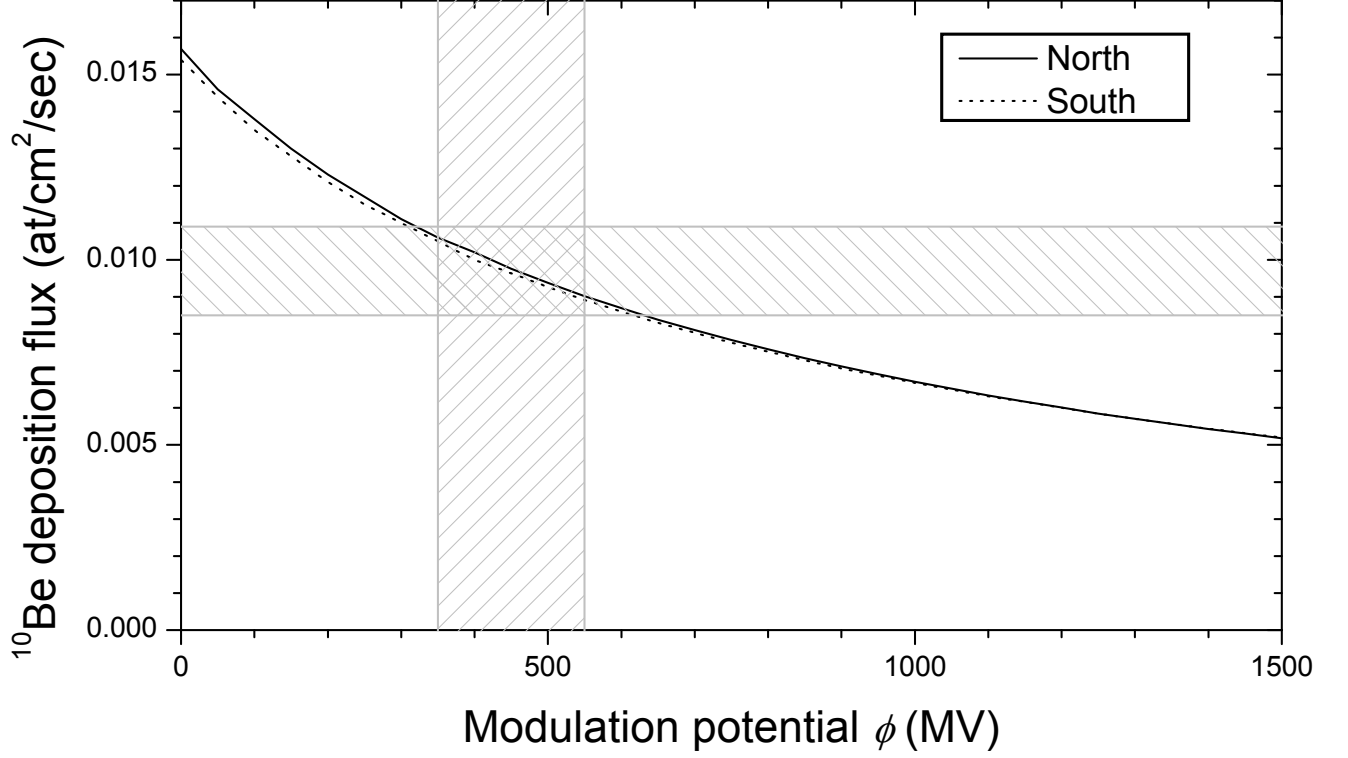


**Figure 9.** Deposition flux of  $^{10}\text{Be}$  in polar regions North and South, as denoted in the legend) computed using the present production model (atmospheric transport was parameterized according to *Heikkilä et al.* [2009]) for the geomagnetic dipole moment,  $M = 10^{23} \text{ A m}^2$  as corresponding to the epoch of 780 AD [*Licht et al.*, 2013]. The horizontal hatched strip corresponds to the range of the decadal-mean measured fluxes of  $^{10}\text{Be}$  for the period 780–800 AD (with the age dating corrected) for four sites: Dome Fuji, Antarctica [*Miyake et al.*, 2015]; WDC/WAIS, Antarctica; NGRIP, Greenland, and NEEM Greenland [for the last three sites see *Sigl et al.*, 2015]. The vertical filled grey bar represents the range of the modulation parameter  $\phi$  reconstructed from  $^{14}\text{C}$  [*Usoskin et al.*, 2016] for the same period 780–790 AD.